Regional Optimum Frequency Analysis of Resting-State fMRI Data for early detection of Alzheimer's disease Biomarkers

Gaurav Garg[1] . Girijesh Prasad[2] . Lalit Garg[3] . Makoto Miyakoshi[4] . Toshiharu Nakai[5] . Damien Coyle[2]

Abstract

The blood-oxygen label dependent (BOLD) signal obtained from functional magnetic resonance images (fMRI) varies significantly among populations. Yet, there is some agreement among researchers over the pace of the blood flow within several brain regions relative to the subject's age and cognitive ability. Our analysis further suggested that regional coherence among the BOLD fMRI voxels belonging to the individual region of the brain has some correlation with underlying pathology as well as cognitive performance, which can suggest potential biomarkers to the early onset of the disease. To capitalise on this we propose a method, called Regional Optimum Frequency Analysis (ROFA), which is based on finding the optimum synchrony frequency observed at each brain region for each of the resting-state BOLD frequency bands (Slow 5 (0.01-0.027Hz), Slow 4 (0.027-0.073Hz) and slow 3 (0.073 to 0.198Hz)), and the whole frequency band (0.01-0.167Hz) respectively. The ROFA is carried out on fMRI data of total 310 scans, i.e., 26, 175 and 109 scans from 21 young-healthy (YH), 69 elderly-healthy (EH) and 33 Alzheimer's disease (AD) patients respectively, where these scans include repeated scans from some subjects acquired at 3 to 6 months intervals. A 10-fold cross-validation procedure evaluated the performance of ROFA for classification between the YH vs EH, YH vs AD and EH vs AD subjects. Based on the confusion-matrix parameters; accuracy, precision, sensitivity and Matthew's correlation coefficient (MCC), the proposed ROFA classification outperformed the state-of-the-art Group-independent component analysis (Group-ICA), Functional-connectivity, Graph metrics, Eigen-vector centrality, Amplitude of low-frequency fluctuation (ALFF) and fractional amplitude of low-frequency fluctuations (fALFF) based methods with more than 94.99% precision and 95.67% sensitivity for different subject groups. The results demonstrate the effectiveness of the proposed ROFA parameters (frequencies) as adequate biomarkers of Alzheimer's disease.

Keywords: functional-MRI (fMRI); resting-state fMRI; frequency-domain analysis, Regional optimum frequency analysis; clustering; Gaussian mixture model; Alzheimer's disease biomarkers**.**

1 Introduction

Age-related changes in brain and cognition functionality have been studied for many years [1]. It is an accepted fact that older adults have reduced memory performance in working memory, verbal ability, and information processing speed [1, 2]. However, some functions remain intact, including knowledge gathered during the lifetime and emotional responses. Before the advancement in computing machines and the invention of magnetic resonance imaging (MRI) and functional MRI (fMRI) devices, it has always been a challenge to understand the anatomical changes and the functional changes in the brain, and how these anatomical changes influence the function of the brain and vice-versa. [3–6].

Gaurav Garg
garg-g@email.ulster.ac.uk, gauravgarg@braina.live

Girijesh Prasad
g.prasad@ulster.ac.uk

Lalit Garg
lalit.garg@um.edu.mt

Makoto Miyakoshi
mmiyakoshi@ucsd.edu

Toshiharu Nakai
toshi@ncgg.go.jp

Damien Coyle
dh.coyle@ulster.ac.uk

[1] Machine Learning Research, BrainAlive Research Pvt. Ltd, Kanpur, India
[2] School of Computing and Intelligent Systems, Magee Campus, Ulster University, Londonderry, NI, United Kingdom
[3] Faculty of Information & Communication Technology, University of Malta, Msida, Malta
[4] Swartz Center for Computational Neuroscience, Institute for Neural Computation, University of California San Diego, San Diego, California, United States
[5] Neuroimaging & Informatics Lab (Niinf), National Centre for Geriatrics and Gerontology (NCGG), Japan

Analysis of resting-state neuroimaging data in many studies has shown a change in the level of signal activation in those showing the signs of neurodegeneration compared to healthy ageing [1]. Here, the decrease in the activation has been defined as 'deactivation' by many researchers. However, some brain regions, which showed a decline in brain activity during resting-state, were found to generate a significant hyperactivation at low-load state, which may be due to the compensatory steps. In contrast, decreased activation was observed for the high precision tasks, which can be a sign of give-up due to the neurodegenerative effects. By recruiting the otherwise undesignated neurons, the compensatory activities lead to 'dedifferentiation' effects in the resting-state brain patterns[1]. Previous studies [7–10] revealed that the most discriminative features for ageing-related motor and memory impairment are predominantly involved in several different resting-state networks (RSNs). These RSNs are ventral and dorsal attention networks (VAN and DAN) and default mode network (DMN). According to the Automatic Anatomic Labelling (AAL) template, 12 brain regions among a total of 45 different regions at the left side of the brain were considered as crucial for resting-state brain analysis (cf. Table 1). Similarly, for the right side of the brain, 12 out of a total of 45 brain regions were considered as crucial [7–9, 11]. These regions were showing significant but slow (< 0.25Hz) rhythmic blood oxygen level-dependent (BOLD) metabolic activity [12] when recorded using Positron Emission Tomography (PET) and functional MRI based neuroimaging techniques [13].

Many studies suggested specific correlations in the brain regions during resting-state [1] as mentioned above. Most standard techniques for identifying such correlations involves calculating the correlation between signals obtained from various distant brain regions to develop some inference about the synchronisation and functional connectivity patterns among them [14]. An approach based on a connectivity network for regions of interest using an Independent Component Analysis (ICA) framework to observe the magnitude of co-activation was found useful to differentiate healthy controls from AD patients [15]. However, this method did not perform well for differentiating mild cognitive impairment (MCI) subjects from age-matched healthy controls. Studies have suggested that MCI subjects are more prone to advance in AD and can be considered as a precursor to AD [16, 17]. An approach applying Group-ICA on the resting-state fMRI data showed some promising connectivity patterns in DMNs [10], VAN and DAN [6, 18, 19], however, only a small dataset was used in these studies. As the computing efficiency has increased exponentially and the time domain analysis alone could not prove sufficiently reliable, the research focus moved to the frequency domain and multivariate time-frequency analyses [20–22]. The Amplitude of Low-Frequency Fluctuation (ALFF) method for frequency domain analysis was developed as a part of REST toolbox [13]. ALFF measures voxels' temporal similarity within a given cluster, in a voxel-wise fashion for the normalised power in the selected interval of frequency bands [23]. It verifies the concept that the brain areas with the highest ALFF are located within the default mode network observed in healthy subjects' resting-state fMRI [13]. A state-of-the-art approach with a large number of classification features based on functional connectivity, functional dynamics, ALFF, and fractional-ALFF has been developed for resting-state fMRI data. Here for the identified features, each methods' performance and their combination were determined [24]. A study based on wavelet transforms [20] showed the causal connectivity patterns across several brain regions within the selected frequency bands. Their method considered a concept based on the variation in BOLD power over time and frequency axes for specific seed voxels and spherical region of interest around the seed voxel. Their study has reported that BOLD power changes in standard frequency bands (Slow-5 to Slow-2) can be related to the fibre connections modelled by Diffusion-Tensor Imaging (DTI) modality [6, 13, 20]. Recently, deep-learning neural network (DNN) based approaches for Alzheimer's biomarkers also gained momentum in finding clinical biomarkers. Due to their proven efficacy in the supervised classification approach, the target objective was defined during training and tested on similar but unknown data [19, 25–27]. However, overfitting of the DNN for given training data makes these methods restricted to specific clinical settings and slight variation in the data features affects the classifier's performance.

Although the methods mentioned above established correlations between BOLD activations in various brain regions, the resulting connectivity patterns were rather coarse and non-specific. Regardless of the classification performance, the all voxel-based multiple-predictors method mentioned in [24] was found to be comprehensive. Notably, the population size considered in the Group-ICA approach was very small. Also, the comparison groups were the severely affected Alzheimer disease patients (AD = 16) with the mean mini-mental state exam (MMSE) score of 12 and the healthy elderly controls (EH = 15, mean MMSE = 29), which may have resulted in a significant classification accuracy [6, 18, 19]. While in [24] subjects number was higher, i.e., AD= 33 with the MMSE score of ≈20.4 and EH = 69 with the MMSE score of ≈27.5. Similar to our study, both these studies evaluate their methods' classification performance for the subject's pathology and use the resting-state fMRI dataset for AD and age-matched healthy controls. Therefore, these studies' methods were compared with our proposed ROFA method and results are given in section 4.

Other methods based on time-frequency analysis consider each band's overall power, regardless of which frequency is supported by the majority of the voxels in a particular region [13, 20–23]. The results suggest that finding the optimally synchronised frequency may help calibrate specific frequencies corresponding to each brain region. Thus, these results highlight systematic changes in the regional frequency in ageing and neurodegeneration. To this end, this paper looks at the changes in the synchrony of several voxels for different frequency values in each brain region and its consistency across several subject groups including young healthy (N=21), AD (N=33) and age-matched elderly control (N=69) subjects.

In section 2, the characteristics of the generated simulated data and real data used in this analysis are discussed. Initially, in subsection 2.2, the data pre-processing steps, including nuisance regression and signal to noise ratio (SNR) improvement, are

outlined. Later in subsection 2.3, mathematical formulation of the ROFA approach is presented. The proposed ROFA approach is formulated to investigate better the resting-state functional data in the frequency domain based on the optimal number of synchronised voxels in each brain region while minimising the phase-matching errors caused in the time domain. In subsection 2.4, the statistical procedures required to test and validate the proposed ROFA algorithms' efficacy are discussed. In Section 3, the results obtained from the application of ROFA on simulated data and real fMRI data are presented. For this purpose, the results are illustrated for three types of test procedures. Using the Mann–Whitney U test with continuity correction, the ROFA observed frequency values are used to find significantly different brain regions for each group of subjects. Second, these ROFA determined frequency values were further tested using *k*-fold cross-validation to identify if these findings can be used to detect the subject's pathological condition. Lastly, the mean frequencies from all the AAL brain regions from different subject groups were taken as reference biomarker frequencies and tested for their classification efficacy among the given subject groups. Section 4 is devoted to discussing the finding with those presented in the available literature, mainly focused on the advantages and limitations of the proposed ROFA approach. Finally, Section 5 presents a brief conclusion identifying the contributions of this paper and possible future work based on this understanding.

TABLE 1
NAME OF THE BRAIN REGIONS* DEFINED IN AAL TEMPLATE [11]

No.	*Regions Name*	*No.*	*Regions Name*
1.	Superior frontal gyrus, dorsolateral	*25.*	Inferior frontal gyrus, orbital part
2.	Middle frontal gyrus	*26.*	**Superior frontal gyrus, medial orbital (SFG_MO)**
3.	Inferior frontal gyrus, opercular part	*27.*	Gyrus rectus
4.	Inferior frontal gyrus, triangular part	*28.*	**Insula (INS)**
5.	Rolandic operculum	*29.*	Anterior cingulate and paracingulate gyri
6.	Supplementary motor area	*30.*	Median cingulate and paracingulate gyri
7.	Superior frontal gyrus, medial	*31.*	**Posterior cingulate gyrus (PCG)**
8.	Cuneus	*32.*	**Parahippocampal gyrus (PHG)**
9.	Lingual gyrus	*33.*	Temporal pole: superior temporal gyrus
10.	Superior occipital gyrus	*34.*	Temporal pole: middle temporal gyrus
11.	**Middle occipital gyrus (MOG)**	*35.*	Olfactory cortex
12.	**Inferior occipital gyrus (IOG)**	*36.*	**Hippocampus (HIP)**
13.	**Fusiform gyrus (FFG)**	*37.*	**Amygdala (AMYG)**
14.	Superior parietal gyrus	*38.*	Caudate nucleus
15.	Inferior parietal	*39.*	Lenticular nucleus, putamen
16.	Supramarginal gyrus	*40.*	**Lenticular nucleus, pallidum (LN_P)**
17.	Angular gyrus	*41.*	Thalamus
18.	Precuneus	*42.*	Precentral gyrus
19.	Paracentral lobule	*43.*	Calcarine fissure and surrounding cortex
20.	Superior temporal gyrus	*44.*	Postcentral gyrus
21.	Middle temporal gyrus	*45.*	**Heschl gyrus (HESG)**
22.	Inferior temporal gyrus	*46.*	Cerebellum (classified differently than first 45 regions)
23.	**Superior frontal gyrus, orbital part (SFG_OP)**	*47.*	Vermis-cerebelli (classified differently than first 45 regions)
24.	Middle frontal gyrus, orbital part		

Abbreviations (in bold) are given to the 12 brain regions of higher importance in the current study.
To denote left and right brain regions respective prefix 'l' and 'r' will be attached to the abbreviations.

2 Materials and Methods

2.1 fMRI Datasets

2.1.1 Simulated fMRI Datasets

A simulated dataset is generated using a sine wave sequence of various frequencies correlated with different cubical blocks as placed in the brain phantom/mask [4, 28]. A set of 110 simulated datasets were generated with SNR values between -10dB and +10dB with a resolution of 2dB [4]. These specific SNRs were achieved by contaminating the generated brain phantom with an appropriate additive white Gaussian noise (AWGN). These datasets have been produced for 140 scans using simulated voxel time-series blocks with repetition (TR) equal to 3,000ms. According to the Nyquist criterion, a frequency can only be recovered without distortion in a bandlimited signal if the sampling frequency is twice or more than the signal's maximum frequency content. Such as in the present case: the voxel time-series signal has been acquired at a repetition time TR of 3000ms or at a sampling frequency $f_s = 1/\mathrm{TR} = 0.33\mathrm{Hz}$. According to the Nyquist sampling criterion, the maximum frequency component which can be recovered without aliasing can be half of the sampling frequency ($f_s / 2$), i.e. $0.33\mathrm{Hz} / (2) = 0.167\mathrm{Hz}$. Therefore, according to the Nyquist sampling criterion, the 0.167Hz is the upper limit of the frequency for the aliasing free recovery of the frequency components. Hence, available limit of 0.167Hz is simulated for 70 frequency values ranging from 2.4mHz to 0.167 Hz [13]. The generated frequency values were padded with the 1260 zero values to make the total data points 1400, and subsequently, from the Nyquist criterion, the possible frequency resolution of 700 points will become 0.24mHz. Here, 700 frequency windows were chosen, because, these are a multiple of the given number of scans which is 140. Here, selecting a frequency window as a multiple of the scans reduces the sudden drift in the values due to aliasing. However, there is a trade-off between the number of frequency windows and the speed of the algorithm. Therefore, a resolution of 0.24mHz was observed as a suitable choice. We have considered 10,000 voxel blocks for each test frequency per phantom volume. Each of the cubical blocks consists of 10,000 voxels was modulated

with sine waves of synchronising test frequency for 2% to 20% (200 to 2,000) voxels, while the remaining voxels were modulated randomly on other available frequencies. Later these 10,000 voxels were contaminated with the AWGN to vary the SNR between -10dB to +10dB. Altogether, there were 110 test cases for simulated data, i.e., ten gradual variations of the percentage of synced frequency voxels, with 11 gradual variations for SNR in each of the selected synced frequency voxels.

2.1.2 Resting-state fMRI Datasets

This analysis has been applied to a total of 310 fMRI scans were available from 123 subjects, i.e. 26, 175 and 109 scans from 21 young healthy (YH), 69 elderly healthy (EH) and 33 Alzheimer's disease (AD) patients respectively. For all the scans, the time of repetition (TR) and the time of echo (TE) were 3000ms and 30ms, respectively. A total of 140 whole-brain scans totalling to 420s (140 x TR) duration for each of the subjects were recorded.

Here, the scans of 21 YH and 18 EH subjects were recorded with a Siemens Magnetom Trio TIM 3T MRI scanner in a total of 46 sessions at Niinf at National Centre for Geriatrics & Gerontology (NCGG), Japan. There were ten young females aged between 21-29 years with an average age of 23.17 years, eleven young males aged between 21-37 with an average age of 23.43 years, eight elderly females with an average age of 68.80 years, and ten elderly males with an average age of 67.00 years. Here one young female had three sessions, three young males and two elderly females had two sessions each, and all others had one session each totalling 46 sessions. These scans had 64x64x39 voxels of thickness 3x3x3.75 mm^3.

The remaining scans were obtained from the online data repository of Alzheimer's disease Neuroimaging Initiative (ADNI). They had 64x64x48 voxels of thickness 3x3x3.3mm^3 These scans were acquired using a Philips Medical Systems Integra 3T MRI scanner. These include 83 scans from 30 EH females with an average age of 73.11 years, 72 scans from 21 EH males with an average age of 76.92 years, 54 scans from 18 AD females with an average age of 73.22 years, and 109 scans from 15 AD males with the average age of 76.23 years [29]. These scans include repeated scans from some subjects acquired at 3-6 months intervals [29].

The mini-mental state examination (MMSE) scores for AD subjects were 12 to 27 for an average of 20.91. All the subjects were instructed to remain in resting-state, but awake and not think anything specific during the data acquisition. Informed consent was taken from all the volunteers according to the protocol approved by the institutional review board.

2.2 Pre-processing

The fMRI data pre-processing is carried out using the Statistical Parametric Mapping (SPM) toolbox [14, 30]. These preparatory steps were very similar to our previous studies [28, 31, 32]. Normalisation was done following the Montreal Neurological Institute (MNI) template. This template is made by anatomically averaging 152 human brains, and then co-registered with the datasets. Normalisation is required to make the head shapes comparable and to verify the statistical significance of the differences between groups. The other steps include re-slicing and re-aligning. Each fMRI data was also normalised to the 91x109x91 voxels per scan with 2x2x2 mm^3 voxel thickness. De-trending was carried out on time-series from all voxels to remove any linear trend caused by changes in the scanner characteristic due to thermal effects or any other reason [33]. As part of data pre-processing, Nuisance regression of fMRI time series data for cardiac and respiratory artefacts was also applied. For this purpose, a principal component analysis (PCA) based method is applied to subtract the whole brain's noise estimates from the noise at each brain region [34, 35].

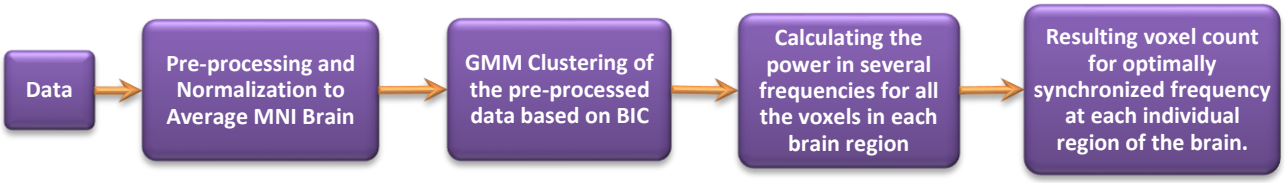

Fig. 1. Calculation Steps of the proposed ROFA with GMM algorithm

2.3 Proposed Regional Optimum Frequency Analysis (ROFA)

After pre-processing the given fMRI data, Gaussian Mixture Model (GMM) based clustering with Bayesian Information Criterion (BIC) was applied to reduce the noise effects from both datasets [5, 28, 31, 36]. In the pre-processed data, consider that $x(n)$ is a time-series, where $n = 1, 2, 3, \dots, N$ corresponding to each voxel (v) from $N = 140$ scans acquired at a sampling interval of 3 second ($f_s = 0.33Hz$). The windowing was applied to this time-series data using Hamming ('bell-shaped') window (W_H) as per (Eq. 1) to enhance the dominating frequency components and reducing the strength of other less dominating frequencies[37]. The Hamming window is a 'bell-shaped' multiplicative function that tapers the sudden changes in the signal time-series and reduces the distorting spikes in the signal time series. The smoothing of edges by the recorded time series's windowing also compensates the fMRI device destabilisation and the brain data's discontinuity [37].

$$x_{NW_H} = x_W(n) = W_H(n).x(n) \qquad (1)$$

The resultant time-series data was transformed into the frequency domain using a Fourier transform (Eq. 2). The magnitude values of the complex-valued Fourier transform were calculated and transformed back to the time domain to remove the phase information (Eq. 3).

$$X_{NW_HK_f} = X_{NW_H}(f_k) = \sum_{n=1}^{n=N} x_{W_H}(n) e^{-\frac{j2\pi f_k n}{f_s}} \qquad (2)$$

$$x_{NW_HK_fM} = x_{NW_HK_fM}(n) = \sum_{k=1}^{k=N} |X_{NW_H}(f_k)| e^{j2\pi f_k n/f_s} \qquad (3)$$

This process was repeated for every voxel ($v = 1, 2, \dots, V$) belonging to each of the brain regions as defined by the selected AAL template, and the mean was calculated over V voxels in a particular brain region (Eq. 4).

$$x_{NW_HK_fMV} = \overline{x_{NW_HK_fM}(v)} = \frac{1}{V}\sum_{v=1}^{v=V} x_{NW_HK_fM}(v) \quad (4)$$

Now, this time-series was padded with zeroes (Eq. 5). In the frequency domain, zero paddings improve the resolution between several different frequencies as observed. In our case, we had *n* = 140 time-points, and we chose to enhance the resolution by ten times, so a total of 1400 time-points were needed. These zeroes are padded to both sides of the signal $x_{NW_HK_fMV}$,

$$x_{NW_HK_fMVZ} = \text{zeroes}(4.5\text{N}) \dots x_{NW_HK_fMV} \dots \text{zeroes}(4.5\text{N}) \quad (5)$$

Then the power spectrum ($\widehat{P(x_{NW_HK_fMVZ})}$) (Eq. 6) was obtained for the whole frequency band from 0.24mHz to 0.167Hz [13, 33, 38].

$$\widehat{P(x_{NW_HK_fMVZ})} = \frac{\left|X_{NW_HK_fMVZ}(f_k)\right|^2}{f_s} \quad (6)$$

Consequently, for the frequency range of 0.24mHz - 0.167Hz, a total of 700 frequency points with a resolution of 0.24mHz were estimated. The first 40 (<0.01Hz) frequency values were discarded, as the frequency values below 0.01Hz are considered to be contaminated with inconsistent human activity, and environmental factors. Hence only the remaining 660 frequency-power values (0.01Hz-0.167Hz) are considered. The power values for each frequency were arranged in ascending order for each interval of frequency bands obtained in each brain region. The optimally synchronised frequency is observed in the given Slow-5: 0.01-0.027Hz, Slow-4: 0.027-0.073Hz, partial Slow-3: 0.073-0.167Hz and the full range of 0.01Hz-0.167Hz, from the available 660 frequency-power components.

$$ROFA_k = \max_k\left(\widehat{P(x_{NW_HK_fMVZ})}\right) \quad (7)$$

Here, $\max_k$ (in Eq. 7) represent the maximum number of voxels collectively giving the optimally synchronized frequency.

This method is based on the maximum number of phase neutralised voxels' time-series showing synchronisation at a particular frequency in a specific region of the brain. Therefore, any drifts in the amplitude of a small proportion of the considered region's voxels do not affect the method. The method's noise robustness has been tested on simulated data consisting of several cases of SNR as low as -10dB (see section 3 and our previous study for details about simulated data generation and noise removal in simulated and real data using GMM [28].

2.4 Statistics

In the simulated data, the original template was available for the optimally synchronised number of voxels for each of the considered frequencies. Therefore, this template was compared with the frequencies obtained after applying the ROFA algorithm in each of the 110 test cases made of 10000 synthetic voxels for 66 different sync frequencies. The obtained results were observed for the percentage of similarity with the template. This comparison, presented in the results section, aimed to validate the proposed ROFA algorithm's efficiency for several test cases.

The real data contained 26 YH, 175 EH and 109 AD datasets from 21, 69 and 33 subjects. Therefore, to avoid any possibility of calculation bias, the repeated scans from the same subjects were handled using a randomising process to analyse only one dataset from each subject. Also, multiple iterations have been used to analyse several different combinations of datasets among those available.

Three types of tests were designed to analyse the statistical significance of ROFA frequency values findings and to estimate their classification performance among healthy and AD subjects. Therefore, in the first test, a one-tailed non-parametric Mann–Whitney U test was utilised to avoid the normality assumption for the data; whereas ROFA frequency values are discrete. Therefore, we have added continuity correction to the obtained statistics for p-value calculation [39]. Here,

$$Z_{continuity\ corrected} = \text{Z}_{stats} \pm \frac{0.5}{\sqrt{\frac{(mn(N+1))}{12}}} \quad (8)$$

where left tail uses $+ve$ sign and right tail uses $-ve$ sign; *m* and *n* ($m \le n$) are the number of observed values in each of the subject groups and $N = m + n$. Z_{stats} is the equivalent z-statistic score on the Gaussian probability curve for the given tail. Furthermore, continuity corrected p-values were calculated in terms of the area under the standard Gaussian probability curve for the obtained $Z_{continuity\ corrected}$.

The continuity correction (Eq. 8) improves the decision making about the significance and avoids the false decision by penalising the p-values. The tail (left or right) was decided based on the mean value of both of the samples under consideration, such as a left tailed test would be selected if the mean of the first sample is less than the second sample and vice-versa. The significance of the alternative hypothesis for regional difference has been established for $p < 0.05$. Literature suggests that the Mann–Whitney U test's test statistics are valid for as small as six samples in each group [39]. A significant difference in ROFA frequency values was observed for each of the AAL regions, as mentioned as important in Table 1. The test was performed on three combinations of

subject pairs YH-EH, YH-AD and EH-AD. This region-wise significance among the given pairs was observed for not only the whole frequency range of 0.01Hz – 0.167Hz but also Slow 5 (0.01-0.027Hz), Slow 4 (0.027-0.073Hz) and partial Slow 3 (0.01-0.167Hz).

The second test is the classification accuracy cross-validation of linear discriminant analysis (LDA). The LDA classifier is selected because this classifier is considered the most suitable classifier than several others such as support vector machine (SVM) and Ensemble learning methods in recent fMRI based AD biomarkers studies [40–42]. The most significant advantage of LDA is that it is fast and robust due to its linear processing structure. Simultaneously, reproducibility is an issue with other complex non-linear classifiers that converge for different solutions every additional time [43]. Another disadvantage of using complex classifiers is identifying the suitable parameters required as *a priori* information, which is not the case with LDA.

For the LDA based classification, the obtained BOLD ROFA frequencies were first randomised from each subject group. Then different subsets of the data were used for training and testing the classification performance. This method gave the classification accuracy based on ROFA values and the loss coefficient for the subjects that failed to be classified accurately based on ROFA frequencies in the available band (0.01Hz-0.167Hz). The loss function was calculated for the data's 10-fold organisation, while the classification accuracy of the randomised sample was calculated for 90% of training and 10% test data. Both the loss function and classification accuracy results were presented as the mean of 100 iterations of each setup. Like the first test, this cross-validation test was also performed on each pair of classes: YH-EH, YH-AD and EH-AD.

The third test was to find the mean of the ROFA frequencies corresponding to all of the AAL regions for each subject group and verify if those mean ROFA frequency values can be used as biomarkers to identify the subject with underlying pathological conditions. For this purpose, a confusion-matrix based approach was developed [28, 31]. The results include the following measures: Accuracy, Precision, Sensitivity and Matthews's correlation coefficient (MCC). MCC coefficient is especially used to estimate the efficiency of the binary classification method [44][22]. These parameters are calculated as per the equations below,

$$Accuracy = \frac{(TP+TN)}{(TP+FP+TN+FN)} \quad (9)$$

$$Precision = \frac{TP}{(TP+FP)} \quad (10)$$

$$Sensitivity = \frac{TP}{(TP+FN)} \quad (11)$$

$$MCC = \frac{((TP\times TN)-(FP\times FN))}{\sqrt{(TP+FP)(TP+FN)(TN+FP)(TN+FN)}} \quad (12)$$

Here, TP, FP, TN and FN are 'true positive', 'false positive', 'true negative' and 'false negative', respectively.

3 RESULTS

3.1 Testing of ROFA on Simulated Data

For this purpose, simulated fMRI datasets were generated, containing the given set of frequencies for gradually varying the percentage of synchronising voxels and the SNR for the signal as described previously in section 2 'Material and Methods'. The ROFA performance is tested concerning the known template of optimally syncing voxels. The test results from the ROFA algorithm on simulated data are shown in Fig. 2.

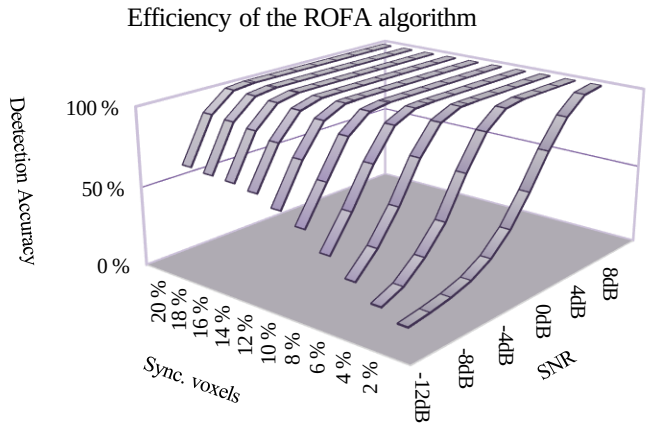

Fig. 2. Percentage efficiency of the ROFA algorithm in detecting the optimally synchronized frequency among the available voxels based on varying SNR and percentage of the synchronized frequencies induced in simulated data.

The obtained ROFA results showed that the efficiency of identifying the optimally syncing frequency increases as the synchronised voxels increase. The ROFA efficiency also improves as the SNR increases. According to our analysis, if 20% of the voxels are contributing to one frequency, then the ROFA can identify the optimally syncing frequency with at least 58.18% accuracy for as low as -10dB SNR, while for SNR higher than -6dB the efficiency can be observed more than 98.40%. Similarly,

suppose the reduction in the percentage of most synchronised voxels is considered. In that case, the ROFA can have an efficiency of 87.82% for 0dB SNR with as low as 4% optimally synchronised voxels. Thus, the algorithm's observed efficiency was more than 74.56% between 8%-20% syncing among voxels for the high noise case of -6dB-10dB. The proposed ROFA algorithm showed even 100% efficiency with an increasing number of synchronising voxels and higher SNR.

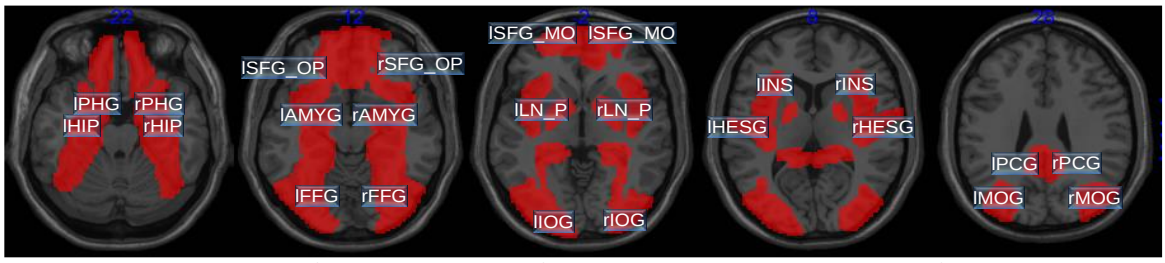

Fig. 3. The 12 regions (counting to 24 regions in left and right brain) selected from the AAL atlas shown above are: Superior frontal gyrus, medial orbital (SFG_MO), Insula (INS), Posterior cingulate gyrus (PCG), Parahippocampal gyrus (PHG), Middle occipital gyrus (MOG), Inferior occipital gyrus (IOG), Fusiform gyrus (FFG), Hippocampus (HIP), Amygdala (AMYG), Lenticular nucleus, pallidum (LN_P), Heschl gyrus (HESG), Superior frontal gyrus, orbital part (SFG_OP).

3.2 ROFA for Real Data

3.2.1 Statistical testing for significantly different brain regions across the groups

We have used the AAL templates available with the MRIcron tool [11, 45]. The AAL template containing 116 regions is selected to analyse the statistical significance of the hypothesis. The hypothesis is that ROFA frequencies of the considered region of the brain belonging to one class of subjects such as EH are significantly different ($p<0.05$) from the same region of the brain belonging to other classes such as AD. However, the concentration was more on the observations from 24 important brain regions (see Fig. 3.) which were suggested as more relevant for investigating differences in the activities of age-related and AD-related brains' activity [7–9, 15, 22]. However, the significant regions among other AAL regions were also estimated. A pairwise analysis strategy was followed to test the statistical significance of the results obtained. For this purpose, the data have been arranged in three groups: 26 Young Healthy/Control (YH), 175 Elderly Healthy/Control (EH) and 109 AD Patients. Here, age-matched male and female subjects are grouped in each of YH, EH and AD groups. Hence the three pairs were formed as YH-EH, YH-AD and EH-AD.

A Mann–Whitney U test with continuity correction [39] was incorporated to penalise the p-value for the discreteness of frequency values and improve the decision making about the significance of the regional difference for standard p ($p< 0.05$). Some of the regions from the selected 24 regions (Fig. 3) from the AAL mentioned in Table 2 were significantly different across the populations [7–9]. We have arranged those regions in the ascending order of their p-values. The significant regions ($p < 0.05$) are presented in boldface. The resting-state fMRI data's regional statistical significance was observed in the slow frequency range of about 0.01Hz – 0.167Hz. This frequency band was further divided in three sub-bands Slow-5 (0.01Hz-0.027Hz), Slow 4 (0.027Hz-0.073Hz) and partial Slow-3 (0.073Hz-0.167Hz) as discussed in section 2.4 "Statistics" [13]. The difference in the mean frequency (FD) is also provided. Table 2 illustrates FD for the Slow-5, Slow-4 and partial Slow-3 bands, while Table 3 shows the same for the whole available band (0.01Hz- 0.167Hz). The FD values (Table 2 & Table 3) were given for all the 24 regions under consideration in a sorted order according to the significance levels' statistical significance. Brain maps in Fig. 4 and Fig. 5 illustrate those brain regions which were found to differ significantly for ($p < 0.05$) among all the available 116 AAL brain regions. Slow 5, slow 4 and slow 3 frequency bands are plotted in Fig. 4(a), (b) & (c), respectively, while Fig. 5 illustrates the significant regions in the whole of the available band. In the given figures (Fig. 4 and Fig. 5) a yellow colour value denotes an increment in the frequency values, while blue colour reduces.

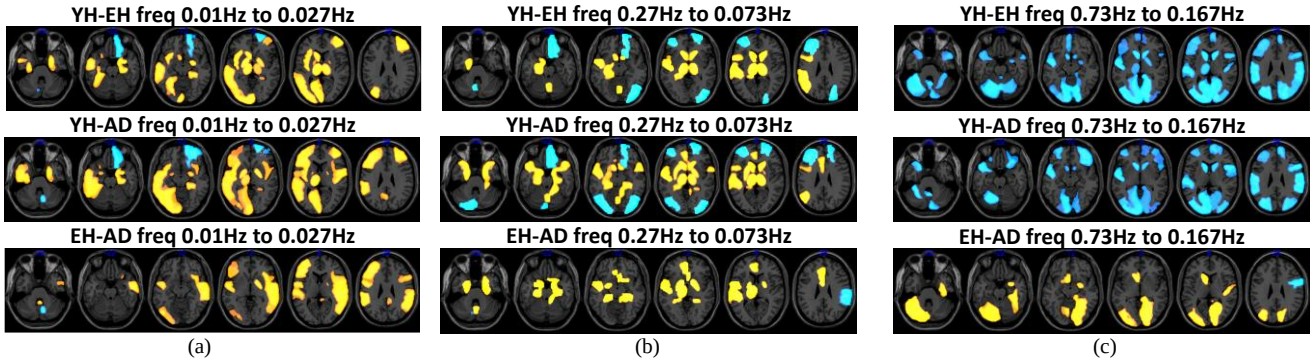

(a) (b) (c)

Fig. 4. Regions observed with significant difference in ROFA activity out of 116 regions in different frequency bands.

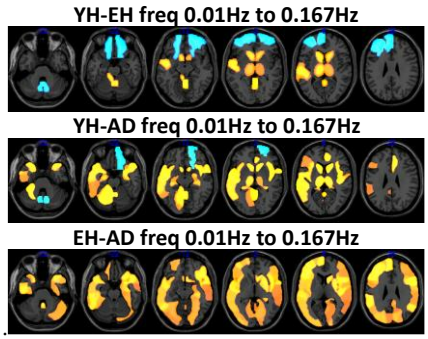

Fig. 5. Regions observed with significant difference in ROFA activity out of 116 regions in whole of the available band. Here yellow colour values denote an increment in the frequency values

TABLE 2
AAL REGIONS* FOR HEALTHY AND AD AFFECTED SUBJECTS

	Significance test for 24 AAL regions using Mann–Whitney U for p < 0.05 (Bold faced)								
	Young (YH) vs Elderly Control (EH)			Young (YH) vs AD Subjects (AD)			Elderly (EH) vs AD Subjects (AD)		
	Region	FD(mHz)*	*p*	Region	FD(mHz)*	*p*	Region	FD(mHz)*	*p*
Slow 5 (0.01↓0.027Hz) or (10-27mHz)	rAMYG	↑3.3	***0.0030***	rLN_P	↑3.5	***0.0010***	rHESG	↑1.6	***0.0053***
	lLN_P	↑3.0	***0.0102***	rPHG	↑3.6	***0.0014***	lIOG	↑1.2	***0.0152***
	rPHG	↑2.4	***0.0172***	rAMYG	↑3.1	***0.0055***	rLN_P	↑1.6	***0.0159***
	rSFG_OP	↓2.2	***0.0344***	lIOG	↑3.1	***0.0056***	rINS	↑1.1	***0.0324***
	rLN_P	↑1.9	***0.0395***	rHESG	↑2.7	***0.0058***	rPCG	↑0.8	***0.0430***
	lFFG	↑1.8	***0.0431***	lFFG	↑2.6	***0.0085***	rPHG	↑1.1	0.0540
	lINS	↑2.1	***0.0458***	rSFG_OP	↓2.1	***0.0131***	lAMYG	↑1.0	0.0774
	lMOG	↑2.1	***0.0469***	lINS	↑2.6	***0.0159***	lFFG	↑0.8	0.1205
	lIOG	↑2.0	0.0615	lLN_P	↑2.9	**0.0165**	lINS	↑0.5	0.1919
	lHIP	↑1.1	0.1113	rINS	↑1.6	**0.0356**	lSFG_MO	↓0.1	0.2268
	lPHG	↑1.0	0.1134	lAMYG	↑1.5	**0.0362**	lPCG	↑0.2	0.2443
	lSFG_OP	↓1.2	0.1370	lMOG	↑2.1	0.0544	rHIP	↑0.5	0.2540
	rHESG	↑1.1	0.1630	lPCG	↑0.7	0.1006	rFFG	↓0.1	0.3181
	rPCG	↓0.5	0.1832	lHIP	↑1.0	0.1260	lSFG_OP	↑0.6	0.3213
	lAMYG	↑0.5	0.1892	lPHG	↑1.0	0.1544	lPHG	↑0.0	0.3308
	lPCG	↑0.5	0.2219	lSFG_OP	↓0.5	0.1618	rMOG	↑0.6	0.3354
	rFFG	↑0.8	0.2285	lHESG	↑0.7	0.2556	rIOG	↑0.3	0.3462
	rINS	↑0.5	0.2471	rHIP	↑1.3	0.2611	rSFG_MO	↓0.1	0.3667
	lSFG_MO	↑0.3	0.2504	rFFG	↑0.7	0.2806	lHESG	↑0.4	0.3712
	lHESG	↑0.2	0.3772	rSFG_MO	↓0.8	0.3027	rAMYG	↓0.2	0.4198
	rSFG_MO	↓0.7	0.3861	lSFG_MO	↑0.2	0.3963	lLN_P	↓0.1	0.4283
	rHIP	↑0.8	0.3917	rMOG	↑0.3	0.4037	lMOG	↑0.0	0.4393
	rMOG	↓0.3	0.5080	rPCG	↑0.2	0.4821	lHIP	↓0.2	0.4582
	rIOG	↑0.1	0.5938	rIOG	↑0.4	0.4911	rSFG_OP	↑0.1	0.6283
Slow 4 (0.027↓0.073Hz) or (27-73mHz)	rIOG	↓7.8	***0.0061***	rIOG	↓8.3	***0.0016***	rLN_P	↑5.9	***0.0006***
	lHIP	↑3.8	***0.0312***	lPHG	↑7.7	***0.0019***	rPHG	↑4.9	***0.0014***
	rSFG_OP	↓6.5	***0.0397***	rSFG_OP	↓8.0	***0.0033***	lAMYG	↑3.3	***0.0065***
	lPHG	↑4.1	***0.0442***	lAMYG	↑4.3	***0.0167***	lLN_P	↑4.0	***0.0081***
	rHIP	↑2.8	0.0541	rPHG	↑8.1	***0.0267***	lPHG	↑3.6	***0.0277***
	lIOG	↓4.1	0.0586	lIOG	↓5.5	***0.0338***	lSFG_OP	↓2.5	0.0558
	rPCG	↓3.1	0.0773	rLN_P	↑4.8	***0.0423***	rSFG_OP	↓1.5	0.0972
	rSFG_MO	↑1.0	0.1808	lHIP	↑3.5	***0.0478***	lMOG	↓1.9	0.1033
	lAMYG	↑1.0	0.2112	lMOG	↓4.3	0.0631	lFFG	↑2.6	0.1064
	lMOG	↓2.4	0.2117	rHIP	↑3.4	0.0806	rAMYG	↑2.4	0.1272
	lFFG	↓2.9	0.2288	lLN_P	↑3.6	0.1327	rINS	↑2.1	0.1687
	rHESG	↓2.1	0.2349	rAMYG	↑4.6	0.1451	lIOG	↓1.5	0.2075
	lSFG_MO	↓2.2	0.2450	lSFG_MO	↓2.7	0.1451	rFFG	↑1.6	0.2077
	rPHG	↑3.1	0.2689	lHESG	↑1.7	0.1671	rPCG	↑0.5	0.2776
	lPCG	↓2.6	0.2877	rPCG	↓2.6	0.1793	rSFG_MO	↓0.7	0.2814
	lHESG	↑0.7	0.2964	rFFG	↑1.7	0.2173	lHESG	↑1.0	0.2869
	rAMYG	↑2.2	0.3008	rINS	↑0.5	0.2264	rIOG	↓0.4	0.3343
	lSFG_OP	↑0.3	0.3128	rHESG	↓1.8	0.2298	lSFG_MO	↓0.5	0.3640
	lINS	↓0.8	0.3435	rSFG_MO	↑0.3	0.2799	rMOG	↓0.5	0.3784
	rFFG	↑0.1	0.3904	lSFG_OP	↓2.2	0.2951	lINS	↑0.6	0.4683
	lLN_P	↓0.4	0.4290	lINS	↓0.1	0.3998	rHESG	↑0.3	0.5056
	rMOG	↑0.5	0.4311	lPCG	↓2.7	0.4412	lHIP	↓0.3	0.5705
	rLN_P	↓1.1	0.4326	lFFG	↓0.3	0.4655	rHIP	↑0.6	0.6454
	rINS	↓1.6	0.4626	rMOG	↑0.0	0.4922	lPCG	↓0.1	0.6686

*FD = Regional difference of mean frequency in mHz, ↓ = reduction and ↑ = increment in frequency of group1 with respect to group2.

TABLE 2
AAL REGIONS* FOR HEALTHY AND AD AFFECTED SUBJECTS

	Significance test for 24 AAL regions using Mann–Whitney U for p < 0.05 (Bold faced)								
	Young (YH) vs Elderly Control (EH)			Young (YH) vs AD Subjects (AD)			Elderly (EH) vs AD Subjects (AD)		
	Region	FD(mHz)*	*p*	Region	FD(mHz)*	*p*	Region	FD(mHz)*	*p*
Partial Slow 3 (0.073↓0.167Hz) or (73-167mHz)	lMOG	↓21.5	***0.0001***	lMOG	↓16.1	***0.0040***	rAMYG	↑7.3	***0.0273***
	rHESG	↓15.3	***0.0053***	rMOG	↓11.4	***0.0344***	rHESG	↑6.4	***0.0293***
	rLN_P	↓11.9	***0.0221***	rSFG_OP	↓11.6	0.0591	rFFG	↑5.9	***0.0316***
	rMOG	↓11.8	***0.0231***	lHESG	↓9.1	0.0670	lMOG	↑5.4	***0.0418***
	lIOG	↓11.0	***0.0370***	rHIP	↑6.2	0.0953	lFFG	↑6.5	0.0515
	lSFG_MO	↓10.8	***0.0425***	rHESG	↓8.9	0.0962	rPHG	↑5.6	0.0583
	rAMYG	↓11.0	***0.0484***	lAMYG	↓11.2	0.1006	lHIP	↑5.1	0.0616
	rSFG_OP	↓12.1	0.0504	rLN_P	↓6.4	0.1021	lIOG	↑5.1	0.0783
	lFFG	↓9.5	0.0555	lSFG_MO	↓8.0	0.1087	rHIP	↑3.8	0.0955
	lPHG	↓11.1	0.0636	rPCG	↓10.0	0.1098	rLN_P	↑5.5	0.0993
	rIOG	↓9.1	0.0767	lSFG_OP	↓8.9	0.1240	lPHG	↑3.7	0.1617
	lHESG	↓6.5	0.1380	rIOG	↓8.1	0.1269	lPCG	↑3.3	0.1682
	lHIP	↓8.5	0.1481	lPHG	↓7.4	0.1438	lAMYG	↓3.4	0.1889
	lAMYG	↓7.8	0.1623	lIOG	↓5.9	0.1523	lLN_P	↑4.5	0.1923
	rFFG	↓5.7	0.1714	rINS	↓3.8	0.1881	rPCG	↓3.8	0.2075
	lINS	↓5.9	0.1812	lLN_P	↑3.5	0.2248	lHESG	↓2.6	0.2144
	lPCG	↓8.5	0.1822	lFFG	↓3.0	0.2256	lSFG_MO	↑2.9	0.2179
	lSFG_OP	↓7.2	0.1885	rSFG_MO	↓3.9	0.2462	lSFG_OP	↓1.7	0.2971
	rPCG	↓6.2	0.1994	lINS	↓5.8	0.2551	rSFG_MO	↓0.1	0.3392
	rHIP	↑2.4	0.2803	rAMYG	↓3.6	0.3146	lINS	↑0.2	0.3778
	rINS	↓3.6	0.2895	rPHG	↑4.0	0.3337	rINS	↓0.3	0.3815
	rPHG	↓1.6	0.3911	rFFG	↑0.2	0.4578	rIOG	↑1.0	0.4278
	rSFG_MO	↓3.8	0.4241	lHIP	↓3.4	0.4911	rMOG	↑0.5	0.4310
	lLN_P	↓1.1	0.5525	lPCG	↓5.3	0.4922	rSFG_OP	↑0.5	0.4751

*FD = Regional difference of mean frequency in mHz, ↓ = reduction and ↑ = increment in frequency of group1 with respect to group2.

TABLE 3
AAL REGIONS* FOR HEALTHY AND AD AFFECTED SUBJECTS

	Significance test for 24 AAL regions using Mann–Whitney U for p < 0.05 (Bold faced)								
	Young (YH) vs Elderly Control (EH)			Young (YH) vs AD Subjects (AD)			Elderly (EH) vs AD Subjects (AD)		
	Region	FD(mHz)*	*p*	Region	FD(mHz)*	*p*	Region	FD(mHz)*	*p*
Whole band (0.01-0.167Hz) or (10-167mHz)	rSFG_OP	↓22.7	***0.0034***	rHESG	↑11.0	***0.0000***	rHESG	↑15.8	***0.0000***
	lSFG_OP	↓19.6	***0.0305***	rAMYG	↑11.3	***0.0006***	rPCG	↑10.0	***0.0005***
	lHIP	↑2.0	0.0662	rSFG_OP	↓18.6	***0.0010***	rINS	↑13.9	***0.0011***
	lAMYG	↑2.4	0.0839	rINS	↑16.5	***0.0020***	rLN_P	↑12.1	***0.0080***
	rPCG	↓7.6	0.1008	lAMYG	↑5.8	***0.0203***	lPCG	↑6.1	***0.0100***
	rSFG_MO	↓9.5	0.1443	lHIP	↑8.5	***0.0206***	lHESG	↑9.2	***0.0119***
	rINS	↑2.7	0.1658	lINS	↑8.7	***0.0263***	rAMYG	↑12.2	***0.0121***
	lHESG	↓9.4	0.2288	lFFG	↑3.8	***0.0269***	lINS	↑12.1	***0.0131***
	rFFG	↓15.3	0.2489	lLN_P	↑3.1	***0.0318***	rPHG	↑9.0	***0.0133***
	rMOG	↓8.8	0.2575	lPCG	↑4.3	***0.0348***	rHIP	↑13.0	***0.0144***
	lMOG	↓11.7	0.3414	rHIP	↑8.1	***0.0392***	lFFG	↑10.2	***0.0188***
	rIOG	↓6.1	0.3711	lPHG	↑1.0	0.1337	lMOG	↑11.2	***0.0207***
	lSFG_MO	↓9.7	0.4297	lSFG_OP	↓8.8	0.1777	lIOG	↑7.6	***0.0224***
	rLN_P	↓13.1	0.5389	rSFG_MO	↓0.9	0.2622	rFFG	↑9.9	***0.0238***
	lIOG	↓8.6	0.5936	rPCG	↑2.4	0.3044	lSFG_OP	↑10.8	***0.0391***
	rHIP	↓4.8	0.6207	rMOG	↓4.7	0.4301	rIOG	↑5.1	0.0804
	lPCG	↓1.8	0.6462	lSFG_MO	↓4.4	0.4522	lAMYG	↑3.4	0.0890
	lINS	↓3.3	0.6821	rIOG	↓1.0	0.7108	lLN_P	↑4.9	0.1586
	rPHG	↓10.1	0.7050	rFFG	↓5.4	0.7521	rSFG_MO	↑8.5	0.1871
	lFFG	↓6.4	0.7074	lHESG	↓0.1	0.7772	rMOG	↑4.1	0.2151
	lPHG	↓1.9	0.8716	lMOG	↓0.5	0.8083	lHIP	↑6.4	0.2229
	lLN_P	↓1.8	0.8991	lIOG	↓1.0	0.9009	lSFG_MO	↑5.3	0.4143
	rHESG	↓4.9	0.9344	rLN_P	↓1.0	0.9698	rSFG_OP	↑4.1	0.5641
	rAMYG	↓0.8	0.9408	rPHG	↓1.1	0.9844	lPHG	↑2.9	0.5926

*FD = Regional difference of mean frequency in mHz, ↓ = reduction and ↑ = increment in frequency of group1 with respect to group2.

Slow 5 bands: In YH vs EH and YH vs AD, the rAMYG and rPHG were commonly found significant (Table 2), which suggests that functional activities at the rPHG and rAMYG have some relation with the age progression, but it does not confirm the significance for any disease related inference. The difference in rPHG was found to be more significant between the YH and AD group than the EH vs AD group, where the frequency was increased more for EH subjects than AD which may infer the age-related increase of BOLD activity in EH subjects. Fig 4(a), depicts that among the other regions the right Insula and frontal inferior triangular gyrus have a significant reduction in the ROFA observed frequency for the AD group. Also, differences in the left Pallidum are more substantial and active in YH than EH and AD.

Slow 4 band: The rPHG, rLN_P and lAMYG (Table 2) and similarly, rLN_P, right olfactory and left anterior Cingulate gyrus in the AD patients (Fig. 4(b)) were found to have significantly lower ROFA values than for the other groups which may relate to disease onset. Other significant regions include lPHG, left Thalamus, left superior temporal lobule (Fig. 4(b)), where the YH group was found to have higher ROFA than both EH and AD patients, which may be an effect of ageing.

Partial Slow 3 band: This band was found to show very different ROFA values than other bands, where almost all of the brain regions were found to have significantly higher BOLD ROFA frequencies than the YH group (Table 2). Interestingly, there was no significant difference between EH and AD except at left and right Postcentral, inferior parietal and Supramarginal gyrus and left Caudate, right Lingual and Calcarine sulcus where EH was observed to have higher ROFA than both YH and AD groups (Fig. 4(c)). These consistently high BOLD ROFA frequencies in the slow 3 band may have some implications to age-related neurodegeneration or age-related increase of BOLD metabolism rate [46][47].

Whole 0.01Hz-0.167Hz band: This band shows considerably more different than other sub-bands because the complete span of the available BOLD ROFA frequency values is analysed in this band. Hence, ROFA values obtained from this band can be considered as an overall ROFA value of the available voxels in a particular brain region. It can be observed from Table 3 that Young brains are resting at relatively lower frequencies than both EH and AD groups. However, a few regions which include right-left Thalamus and Caudate nucleus (Fig. 5.) are found to have a significantly higher ROFA frequency than EH and AD groups. It can also be hypothesised that ROFA frequency for Elderly brain is generally higher than both Alzheimer's patients and young, healthy subjects, which is in coherence with the large study depicting the age-related increase of the cerebral metabolic rate of oxygen consumption ($CMRO_2$) [46].

Table 4

Loss function for *k*-fold cross-validation among different subject groups for k = 10			
Subject group	**YH-EH**	**YH-AD**	**EH-AD**
Loss coefficient	0.19	0.33	0.29

Table 5

Cross validation accuracy among different subject groups for several different combinations of 90% of the training and 10% test data.			
Subject group	**YH-EH**	**YH-AD**	**EH-AD**
Prediction accuracy	76.10%	67.55	68.09%

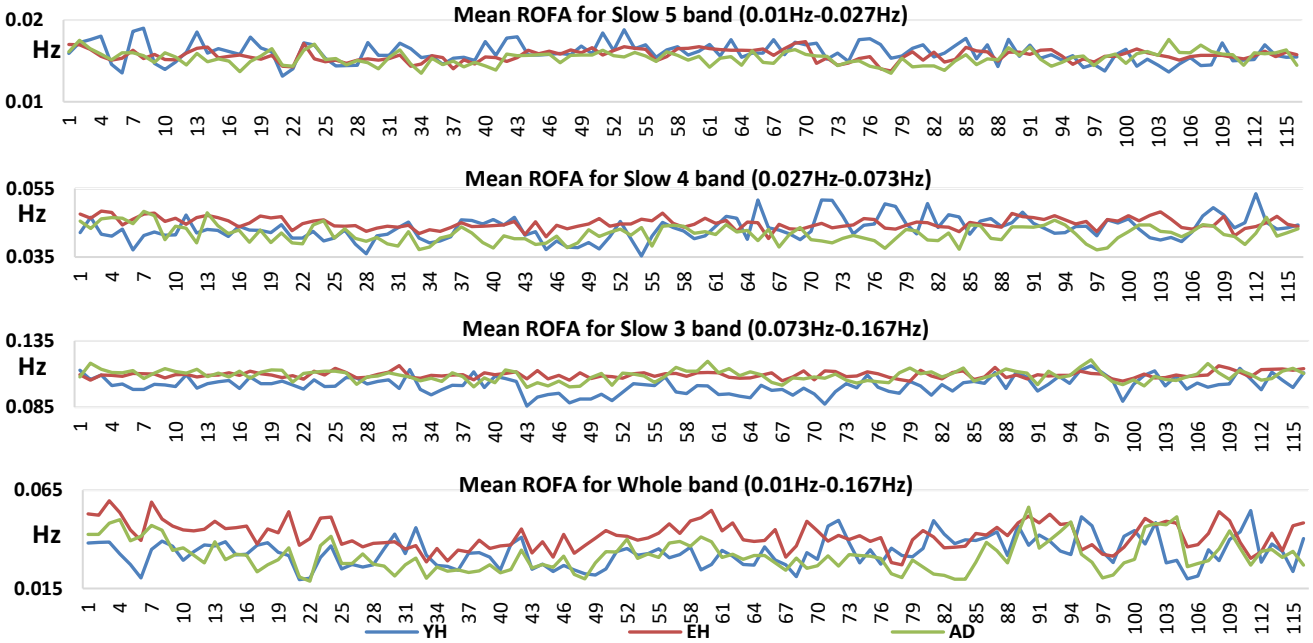

Fig. 6. Mean of the observed BOLD ROFA frequencies in the selected bands for each of the 116 brain regions for Young healthy, Elderly healthy and Alzheimer's disease group.

3.2.2 Cross-validation of ROFA generated frequencies to test their affinity with their group

We have used the data in a linear discriminant analysis (LDA) based classifier with the loss function test for the10 folds cross-validation. Each of the loss function results was randomised and averaged from 100 iterations each. The loss function assesses the efficiency of the suggested features, which in our case are the BOLD ROFA frequencies for the whole band (0.01Hz-0.167Hz) as observed for 116 AAL brain regions in all 123 subjects. Here we randomly selected only one dataset from each subject (for those subjects with multiple datasets) to remove any possibility of bias due to longitudinal data from the same subject. This randomisation was also done for 100 observations. Table 4 illustrates the observed results for the loss-function coefficients, which can have a

value between 0 and 1. This value suggests the ratio of the data which failed to classify well by the classifier. As can be seen from Fig.6, the loss was low < 0.19 for the YH-EH comparison, while for YH-AD and EH-AD groups the loss coefficient was about 0.33 and 0.29, respectively, across all the different data-fold combinations for training and testing.

As described in Section 2.4, these features were further tested for the classification accuracy in the same LDA-based classifier with a slightly different setup for training and testing data. Here, data from each of the subject groups were divided using a randomisation algorithm and fed to the classifier in equal proportion from each YH, EH and AD groups. The classification results for this cross-validation approach are also significant (Table 7.) and adhere to the findings of the loss function. Here the predictability accuracy was 76.10% for YH-EH, while for YH-AD and EH-AD the accuracy was up to 67.55% and 68.09%, respectively.

Table 6

Kendall's rank correlation coefficients $\boldsymbol{r}$ among mean ROFA values along with their p-values

	YH-EH		YH-AD		EH-AD	
	r	p_val	r	p_val	r	p_val
Slow 5 band	0.2414	0.0344	0.1058	0.0813	0.2690	0.0159
Slow 4 band	0.0051	0.3121	0.0081	0.1673	0.3343	0.0651
Slow 3 band	0.1499	0.0231	0.1352	0.0344	0.1421	0.0316
Whole band	0.1439	0.0305	0.1199	0.0206	0.5478	0.0121

3.3 ROFA frequencies as biomarkers for ageing and pathological changes in the brain

The mean ROFA frequencies have been calculated for each of the 116 brain regions across the subject groups for all of the discussed frequency bands (see Fig. 6.). Then, the similarities in the mean frequency values of different subject groups were observed. Though between-subject variability may be high, the pattern should be similar in each population group. Therefore, a non-parametric Kendall's rank correlation was considered appropriate because the Kendall rank correlation is considered more sensitive to pattern differences in the given data samples [39]. Interestingly, frequency correlations given in Table 6 can also validate the difference between AD and YH subjects in all four frequency bands. The correlation (see Table 6) between YH and EH subjects was observed as $r = 0.2414, 0.0051, 0.1499\ and\ 0.1439$. It is undoubtedly better than that in YH-AD where $r = 0.1058, 0.0081, 0.1352\ and\ 0.1199$. It also makes sense that the correlation for EH-AD ($r = 0.2690, 0.3343, 0.1421\ and\ 0.5478$) have highest similarity in the ROFA patterns for each frequency band, as both EH & AD groups have similar age profile. Moreover, these results are thoroughly coherent with several frequency bands under consideration.

The mean frequency values (Fig. 6.) were further tested to infer the subject groups and underlying pathological conditions. The distance or affinity to these mean frequency values was observed. All of the 123 subjects and findings were arranged in the confusion-matrix based test statistics. For this purpose, Accuracy, Precision, Sensitivity and Matthew's Coefficient of correlation (MCC) were calculated as explained in Section 2.4 and (1) to (4), respectively. The results presented in Table 7 are organised such as for the first row 'YH-EH', YH has been considered True Positive (TP) group and EH as True Negative (TN) group and similarly for remaining 5 rows. Table 8 has been derived from Table 7, which provides the mean results for both groups after swapping between TP and TN. For example, the first row is the mean of YH-EH and EH-YH observations. All of the results are scaled to an equal number of subjects from each group and projected to contain 1,000 subjects in each group totalling to 3,000 subjects for YH, EH, and AD to remove any possibility of bias.

Table 7

Observations made from the Confusion-Matrix results

	Accuracy	Precision	Sensitivity	MCC
YH-EH	95.71%	92.47%	100%	95.97%
YH-AD	100%	100%	100%	100%
EH-AD	94.99%	100%	89.98%	95.32%
EH-YH	95.71%	100%	91.42%	95.97%
AD-YH	100%	100%	100%	100%
AD-EH	94.99%	91.33%	100%	95.32%

Table 8

Mean of the Confusion-Matrix results of the Table VIII

	Accuracy	Precision	Sensitivity	MCC
YH-EH	95.71%	96.24%	95.71%	95.97%
YH-AD	100%	100%	100%	100%
EH-AD	94.99%	95.67%	94.99%	95.32%

This can be inferred from Table 8 that there is up to 95.71% accuracy of detection for Young Healthy subjects. At the same time, for Elderly and Alzheimer's (EH-AD & AD-EH), the ROFA frequencies were able to identify 94.99% of subjects correctly for their groups. It is even more interesting to observe the sensitivity values, suggesting having separated all 100% of the Young Healthy subjects from both Elderly and Alzheimer's group. It is conceptually true as young brains are unlikely to have

neurodegenerative effects observed from ageing and Alzheimer's disease. However, a very small number of Elderly (8.58%) subjects were found to have similar responses as YH subjects. These results prove obvious that EH brains are healthier than AD. Therefore few of the EH subjects may have similar BOLD ROFA responses as the YH subjects, while the AD patients are not similar to YH brains. On comparing the difference between detectability of AD among the elderly population, 10.02% of elderly healthy subjects were found to fall in the AD category. Studies by Koch et al., 2012 and Prvulovic et al., 2011 [15, 22] suggest that logically these fallout cases are appropriate because Elderly healthy and AD patients belong to similar age group. They may have more similarities than differences, and therefore a few Elderly subjects have been suggested to have Alzheimer's disease. This fallout of EH subjects as AD might be an initial indicator of AD or other similar neurodegenerative diseases in these subjects. Hence, such cases may also be opinionated to keep monitoring their cognitive, memory and emotional performance.

Table 9

Comparison of proposed ROFA method with Group-ICA method and a method based on the combination of Functional connectivity, Graph Metrics, Eigen Vector Centrality, ALFF and fALFF methods.

Method used (groups)	Regions selected	No. of Subjects (Average MMSE)	Efficiency Sens./Prec.%
Group-ICA [6, 18, 19, 27]			
EH vs. AD	DMN Regions DAN Regions VAN Regions	EH = 16 (≈29) AD = 15 (≈12)	73.3–86.7/NA 85.7–100/NA <70–73.3/NA
Classification using Functional connectivity, Graph Metrics, Eigen Vector Centrality, ALFF and fALFF methods [24].			
EH vs. AD	Individual Methods Combined	EH = 69 (≈20.4) AD = 33 (≈27.5)	46-84/50-76 86/75
Proposed Regional Optimum Frequency Analysis (ROFA)			
YH vs. EH YH vs. AD EH vs. AD	Whole Brain (AAL) [11]	YH = 21 (NA*) EH = 69 (>27) AD = 33 (≈21)	95.71/96.24 100/100 94.99/95.67

**MMSE test for young healthy subjects was not done.*

4 Discussion

Though anatomical relevance is useful in understanding neurodegenerative diseases, especially Alzheimer's disease, and may have a definite impact on the pathological calibration of diseases [1, 2, 48], the focus of this study remained on the BOLD spontaneity of brain regions [4, 13, 23, 28, 31]. Therefore, anatomical relevance has been considered up to normalisation with MNI templates [30]. Thus, this study's anatomical accuracy relies on the efficiency of the existing pre-processing algorithms as provided by the SPM toolbox for MATLAB [30].

The proposed ROFA methods have found several regions showing significant differences ($p < 0.05$) in optimum frequency using non-parametric Mann–Whitney U test [39]. The detailed exploration of these outcomes' biological significance is out of the scope of this work. However, the results demonstrate that some regions have shown a reduction in frequency for elderly controls and AD patients, which may be due to the slowing of the ageing brain, reduction in oxygenated blood supply or reduced network connections. Also, there was some increase in frequency in a few brain regions that may be considered a consequence of the scaffolding or the compensation mechanism for the regions with deteriorated functionality due to ageing and/or AD-related pathological changes [1, 46]. A comparison of the proposed ROFA with promising Group-ICA based method is given in Table 9. Group-ICA achieved 100% classification sensitivity for connectivity pattern in the dorsal attention network (DAN). Still, the MMSE-Score for the selected AD subjects suggest, the AD patients were severely affected. At the same time, our study considered several different AD patients from mild (MMSE ≈ 26) to severe (MMSE ≈ 12) conditions. The classification robustness of these ROFA algorithms was tested on simulated and Real fMRI datasets in the present study and GMM from our previous study [28, 31] has been used for SNR improvement. We have found GMM along with ROFA approach as suitable to deploy for both resting-state and stimulus-dependent fMRI data analysis with the following limitations, 1) the outcome of the ROFA would remain prone to motion and normalisation artefacts [4] which depends on the accuracy of pre-processing tools such as SPM [30] in our case, 2) GMM is based on an expectation-maximisation algorithm which needs relatively more computing power as well as time, 3) ROFA algorithms suppress the amplitude information from the fMRI data and so the significance is limited to the functional spontaneity or the pace of the BOLD fluctuations only.

The main advantages of using these algorithms are: 1) noise robustness due to Bayesian information criterion [5] based clustering, 2) the ROFA algorithm works in the frequency domain and therefore drift caused due to phase differences in chaotic time-series signals get minimised, 3) the ROFA algorithm being based on a huge number of optimally synced voxels can deal better with significantly random nature of the brain signals and 4) the ROFA algorithm counts on the relative differences in the group of voxels syncing for a frequency of the subject's brain. Therefore, it is relatively independent to the device environment artefacts.

This method may potentially establish reliable biomarkers for normal healthy ageing and neurodegenerative disorders. Thanks to their noise robustness, accuracy and reproducibility of the outcomes. The results obtained from ROFA are considerably different than many other methods which consider BOLD power in the suggested bands of frequencies. The ROFA considers the optimal number of voxels synced to a particular BOLD frequency regardless of the strength or power in other bands for relatively fewer synced voxels. Here, a group analysis strategy was opted to determine the difference between healthy age groups and AD patients. The proposed algorithm has identified differences between healthy, elderly and AD brains. The most adherent frequency for each brain region among the given young, elderly and AD groups can be depicted from the findings. Earlier findings based on frequency analysis have also established that fMRI BOLD responses can be used to differentiate between the healthy and diseased brain. In contrast, the proposed ROFA algorithm has been tested to find the ageing-related changes and the disease, which proves the algorithm's legitimacy per the available literature[23, 49–54].

5 Conclusion and future work

This paper has presented a novel approach based on the optimally synchronised frequency response of the recorded BOLD fMRI voxels belonging to a particular region of the brain, namely ROFA. This algorithm was successfully applied to the resting-state data from young and elderly healthy control subjects and Alzheimer's disease patients and tested for statistical significance in a group analysis model. Some regions have shown BOLD variability in the form of optimum resting frequency using ROFA for several brain regions as classified by AAL brain atlas template obtained from the MRIcron software [45]. Our method's efficacy was tabulated for 24 essential regions of the brain, as suggested in the literature, although results were analysed for other brain regions. The ROFA frequencies for Young healthy subjects showed a higher correlation with AD subjects in lower frequency (< 027Hz) band while Elderly healthy found to have higher correlation is relatively higher frequency (>0.27Hz) bands. Further, the ROFA frequencies were tested for their candidature as biomarkers to observe the brain's pathological state. A confusion-matrix based statistics was incorporated for this purpose, and the results were validated on the Accuracy, Precision, Sensitivity and Matthews Coefficient of Correlation (MCC) parameters. Here, the ROFA values were able to identify young, healthy subjects with 100% Accuracy and Precision both, while Elderly healthy and AD subjects were also separated with more than 96% precision and nearly 95% accuracy. With these values, ROFA outperformed the Group-ICA[18, 19] and recent multi-classifier based functional connectivity, graph metrics, Eigen-vector centrality, ALFF and fALFF based methods[24]. This proves the superiority of the ROFA method in differentiating into healthy ageing individuals and AD subjects.

Acknowledgements

The Computational Neuroscience Research Team supported this work under the N. Ireland Department for Education and Learning – "Strengthening the All-island Research Base" project.

Alzheimer's disease data used in this article's preparation were obtained from the Alzheimer's Disease Neuroimaging Initiative (ADNI) database (adni.loni.ucla.edu).

References

1. Grady C (2012) The cognitive neuroscience of ageing. Nat Rev Neurosci 13:491–505. https://doi.org/10.1038/nrn3256
2. Schroeter ML, Stein T, Maslowski N, Neumann J (2009) Neural correlates of Alzheimer's disease and mild cognitive impairment: a systematic and quantitative meta-analysis involving 1351 patients. Neuroimage 47:1196–1206. https://doi.org/10.1016/j.neuroimage.2009.05.037
3. Chen C-CC, Tyler CCW (2008) Spectral Analysis of fMRI Signal and Noise. Springer Japan, Tokyo
4. Dimitriadou E, Barth M, Windischberger C, et al (2004) A quantitative comparison of functional MRI cluster analysis. Artif Intell Med 31:57–71. https://doi.org/10.1016/j.artmed.2004.01.010
5. Fonseca JRS (2008) The application of mixture modeling and information criteria for discovering patterns of coronary heart disease. J Appl Quant Methods 3:292–303
6. Li R, Wu X, Fleisher AS, et al (2012) Attention-related networks in Alzheimer's disease: a resting functional MRI study. Hum Brain Mapp 33:1076–1088. https://doi.org/10.1002/hbm.21269
7. Chetelat G aë., Baron J-C (2003) Early diagnosis of alzheimer's disease: contribution of structural neuroimaging. Neuroimage 18:525–541. https://doi.org/10.1016/S1053-8119(02)00026-5
8. Baron JC, Chételat G, Desgranges B, et al (2001) In vivo mapping of gray matter loss with voxel-based morphometry in mild Alzheimer's disease. Neuroimage 14:298–309. https://doi.org/10.1006/nimg.2001.0848
9. Dai Z, Yan C, Wang Z, et al (2012) Discriminative analysis of early Alzheimer's disease using multi-modal imaging and multi-level characterisation with multi-classifier (M3). Neuroimage 59:2187–95. https://doi.org/10.1016/j.neuroimage.2011.10.003
10. Raichle ME, MacLeod a M, Snyder a Z, et al (2001) A default mode of brain function. Proc Natl Acad Sci U S A 98:676–82. https://doi.org/10.1073/pnas.98.2.676
11. Tzourio-Mazoyer N, Landeau B, Papathanassiou D, et al (2002) Automated anatomical labeling of activations in SPM using a macroscopic anatomical parcellation of the MNI MRI single-subject brain. Neuroimage 15:273–289. https://doi.org/10.1006/nimg.2001.0978
12. Buxton RB, Wong EC, Frank LR (1998) Dynamics of blood flow and oxygenation changes during brain activation: The balloon model. Magn Reson Med 39:855–864. https://doi.org/10.1002/mrm.1910390602
13. Yang H, Long X-Y, Yang Y, et al (2007) Amplitude of low frequency fluctuation within visual areas revealed by resting-state functional MRI. Neuroimage 36:144–52. https://doi.org/10.1016/j.neuroimage.2007.01.054
14. Friston KJ, Holmes AP, Worsley KJ, et al (1994) Statistical parametric maps in functional imaging: A general linear approach. Hum Brain Mapp

2:189–210. https://doi.org/10.1002/hbm.460020402
15. Koch W, Teipel S, Mueller S, et al (2012) Diagnostic power of default mode network resting state fMRI in the detection of Alzheimer's disease. Neurobiol Aging 33:466–78. https://doi.org/10.1016/j.neurobiolaging.2010.04.013
16. Binnewijzend M a a, Schoonheim MM, Sanz-Arigita E, et al (2012) Resting-state fMRI changes in Alzheimer's disease and mild cognitive impairment. Neurobiol Aging 33:2018–28. https://doi.org/10.1016/j.neurobiolaging.2011.07.003
17. Liu Y, Yu C, Zhang X, et al (2014) Impaired long distance functional connectivity and weighted network architecture in Alzheimer's disease. Cereb Cortex 24:1422–35. https://doi.org/10.1093/cercor/bhs410
18. Fiandaca MS, Mapstone ME, Cheema AK, Federoff HJ (2014) The critical need for defining preclinical biomarkers in Alzheimer's disease. Alzheimers Dement 10:S196-212. https://doi.org/10.1016/j.jalz.2014.04.015
19. Duc NT, Ryu S, Qureshi MNI, et al (2020) 3D-Deep Learning Based Automatic Diagnosis of Alzheimer's Disease with Joint MMSE Prediction Using Resting-State fMRI. Neuroinformatics 18:71–86. https://doi.org/10.1007/s12021-019-09419-w
20. Bajaj S, Adhikari BM, Dhamala M (2013) Higher frequency network activity flow predicts lower frequency node activity in intrinsic low-frequency BOLD fluctuations. PLoS One 8:e64466. https://doi.org/10.1371/journal.pone.0064466
21. Hampel H, Frank R, Broich K, et al (2010) Biomarkers for Alzheimer's disease: academic, industry and regulatory perspectives. Nat Rev Drug Discov 9:560–574. https://doi.org/10.1038/nrd3115
22. Prvulovic D, Bokde ALW, Faltraco F, Hampel H (2011) Functional magnetic resonance imaging as a dynamic candidate biomarker for Alzheimer's disease. Prog Neurobiol 95:557–69. https://doi.org/10.1016/j.pneurobio.2011.05.008
23. Salvador R, Martínez A, Pomarol-Clotet E, et al (2007) Frequency based mutual information measures between clusters of brain regions in functional magnetic resonance imaging. Neuroimage 35:83–88. https://doi.org/10.1016/j.neuroimage.2006.12.001
24. de Vos F, Koini M, Schouten TM, et al (2018) A comprehensive analysis of resting state fMRI measures to classify individual patients with Alzheimer's disease. Neuroimage 167:62–72. https://doi.org/10.1016/j.neuroimage.2017.11.025
25. Parmar H, Nutter B, Long R, et al (2020) Spatiotemporal feature extraction and classification of Alzheimer's disease using deep learning 3D-CNN for fMRI data. J Med Imaging 7:. https://doi.org/10.1117/1.JMI.7.5.056001
26. Basaia S, Agosta F, Wagner L, et al (2019) Automated classification of Alzheimer's disease and mild cognitive impairment using a single MRI and deep neural networks. NeuroImage Clin 21:101645. https://doi.org/10.1016/j.nicl.2018.101645
27. Qureshi MNI, Ryu S, Song J, et al (2019) Evaluation of Functional Decline in Alzheimer's Dementia Using 3D Deep Learning and Group ICA for rs-fMRI Measurements. Front Aging Neurosci 11:. https://doi.org/10.3389/fnagi.2019.00008
28. Garg G, Prasad G, Coyle D (2013) Gaussian mixture model-based noise reduction in resting state fMRI data. J Neurosci Methods 215:71–77. https://doi.org/10.1016/j.jneumeth.2013.02.015
29. Weiner MW, Veitch DP, Aisen PS, et al (2012) The Alzheimer's Disease Neuroimaging Initiative: a review of papers published since its inception. Alzheimer's Dement 8:S1-68. https://doi.org/10.1016/j.jalz.2011.09.172
30. Ashburner J, Barnes G, Chen C-C, et al (2012) SPM8 Manual The FIL Methods Group (and honorary members). Functional Imaging Laboratory, Wellcome Trust Centre for Neuroimaging, Institute of Neurology, UCL, London, UK
31. Garg G, Prasad G, Garg L, Coyle D (2011) Gaussian mixture models for brain activation detection from fmri data. Int J Bioelectromagn 13:255–60
32. Garg L, McClean S, Meenan B, et al (2009) Clustering patient length of stay using mixtures of Gaussian models and phase type distributions. In: 22nd IEEE International Symposium on Computer-Based Medical Systems2nd IEEE International Symposium on Computer-Based Medical Systems. IEEE, Albuquerque, NM, pp 1–7
33. Song X-W, Dong Z-Y, Long X-Y, et al (2011) REST: a toolkit for resting-state functional magnetic resonance imaging data processing. PLoS One 6:e25031. https://doi.org/10.1371/journal.pone.0025031
34. Chai XJ, Castañón AN, Ongür D, Whitfield-Gabrieli S (2012) Anticorrelations in resting state networks without global signal regression. Neuroimage 59:1420–8. https://doi.org/10.1016/j.neuroimage.2011.08.048
35. Hayasaka S (2013) Functional connectivity networks with and without global signal correction. Front Hum Neurosci 7:880. https://doi.org/10.3389/fnhum.2013.00880
36. Challis E, Hurley P, Serra L, et al (2015) Gaussian process classification of Alzheimer's disease and mild cognitive impairment from resting-state fMRI. Neuroimage 112:232–243. https://doi.org/10.1016/j.neuroimage.2015.02.037
37. Spangenberg S, Scott I, McLaughlin S, et al (2000) An FFT-Based Approach for Fast Acquisition in Spread Spectrum Communication Systems. Wirel Pers Commun 13:27–55. https://doi.org/10.1023/A:1008848916834
38. Welch P (1967) The use of fast Fourier transform for the estimation of power spectra: A method based on time averaging over short, modified periodograms. IEEE Trans Audio Electroacoust 15:70–73. https://doi.org/10.1109/TAU.1967.1161901
39. Gibbons J, Chakraborti S (2011) Nonparametric Statistical Inference. Springer Berlin Heidelberg, Berlin, Heidelberg
40. Coupé P, Eskildsen SF, Manjón J V., et al (2012) Scoring by nonlocal image patch estimator for early detection of Alzheimer's disease. NeuroImage Clin 1:141–152. https://doi.org/10.1016/j.nicl.2012.10.002
41. Wolz R, Julkunen V, Koikkalainen J, et al (2011) Multi-Method Analysis of MRI Images in Early Diagnostics of Alzheimer's Disease. PLoS One 6:e25446. https://doi.org/10.1371/journal.pone.0025446
42. Liu M, Zhang D, Shen D (2014) Identifying Informative Imaging Biomarkers via Tree Structured Sparse Learning for AD Diagnosis. Neuroinformatics 12:381–394. https://doi.org/10.1007/s12021-013-9218-x
43. Griffanti L, Rolinski M, Szewczyk-Krolikowski K, et al (2016) Challenges in the reproducibility of clinical studies with resting state fMRI: An

example in early Parkinson's disease. Neuroimage 124:704–713. https://doi.org/10.1016/j.neuroimage.2015.09.021

44. Carugo O (2007) Detailed estimation of bioinformatics prediction reliability through the Fragmented Prediction Performance Plots. BMC Bioinformatics 8:380. https://doi.org/10.1186/1471-2105-8-380
45. Rorden C, Brett M (2000) Stereotaxic display of brain lesions. Behav Neurol 12:191–200
46. Peng S-L, Dumas JA, Park DC, et al (2014) Age-related increase of resting metabolic rate in the human brain. Neuroimage 98:176–83. https://doi.org/10.1016/j.neuroimage.2014.04.078
47. Dørum ES, Kaufmann T, Alnæs D, et al (2017) Increased sensitivity to age-related differences in brain functional connectivity during continuous multiple object tracking compared to resting-state. Neuroimage 148:364–372. https://doi.org/10.1016/j.neuroimage.2017.01.048
48. Lemaître H, Crivello F, Grassiot B, et al (2005) Age- and sex-related effects on the neuroanatomy of healthy elderly. Neuroimage 26:900–911. https://doi.org/10.1016/j.neuroimage.2005.02.042
49. Riedl V (2012) Intrinsic functional brain networks in health and disease
50. Cole DM, Smith SM, Beckmann CF (2010) Advances and pitfalls in the analysis and interpretation of resting-state FMRI data. Front Syst Neurosci 4:8. https://doi.org/10.3389/fnsys.2010.00008
51. Greicius MD, Supekar K, Menon V, Dougherty RF (2009) Resting-state functional connectivity reflects structural connectivity in the default mode network. Cereb Cortex 19:72–8. https://doi.org/10.1093/cercor/bhn059
52. Hoptman MJ, Zuo X-N, Butler PD, et al (2010) Amplitude of low-frequency oscillations in schizophrenia: a resting state fMRI study. Schizophr Res 117:13–20. https://doi.org/10.1016/j.schres.2009.09.030
53. Fox MD, Raichle ME (2007) Spontaneous fluctuations in brain activity observed with functional magnetic resonance imaging. Nat Rev Neurosci 8:700–11. https://doi.org/10.1038/nrn2201
54. Mezer A, Yovel Y, Pasternak O, et al (2009) Cluster analysis of resting-state fMRI time series. Neuroimage 45:1117–25. https://doi.org/10.1016/j.neuroimage.2008.12.015